FHR Core Monte Carlo Calculation using Serpent2 Code

Davor Grgić, Radomir Ječmenica
University of Zagreb Faculty of Electrical Engineering and Computing
Unska 3, 10000 Zagreb, Croatia
Davor.Grgic@fer.unizg.hr, Radomir.Jecmenica@fer.unizg.hr

Bojan Petrović
Georgia Institute of Technology
Atlanta, GA, USA
Bojan.Petrovic@gatech.edu

ABSTRACT

Steady-state neutronic calculations for the OECD/NEA Fluoride-salt-cooled High-temperature Reactor (FHR)/Advanced High-Temperature Reactor (AHTR) Benchmark – Phase II-A are presented. The analysis was performed using continuous-energy Monte Carlo code Serpent 2.2.3 on a full-core model derived from a modified ORNL AHTR reference design. This study specifically addresses Exercise 1, providing a foundational characterization of the system's neutronic parameters, including the effective multiplication factor (k_{eff}), fission rate density distributions, total and three-group neutron flux, and the neutron energy spectrum. Neutron flux distributions were resolved at both the fuel assembly level and on a high-resolution three-dimensional Cartesian mesh. A systematic evaluation of the convergence behavior was conducted, focusing on the influence of active generations and particle histories on the spatial distribution of flux uncertainties. The calculated distributions were rigorously assessed for radial and axial symmetry. Furthermore, methodologies for spatial and energy flux collapsing – implemented both through internal detector definitions and external post-processing – were evaluated. These results establish a high-fidelity baseline for code-to-code comparison within the FHR/AHTR benchmark framework.

Keywords: *FHR core calculation, Monte Carlo criticality, Serpent2 code*

1 INTRODUCTION

The Fluoride-salt-cooled High-temperature Reactor (FHR) is an advanced nuclear energy system characterized by the integration of TRISO-based fuel, graphite moderation, and the superior heat-transfer properties of molten fluoride salts [6][7]. To ensure the reliability of computational tools for the safety and performance analysis of such systems, the OECD Nuclear Energy Agency (NEA) has established a multi-phase benchmark framework. This benchmark is based on the Advanced High-Temperature Reactor (AHTR) conceptual design, originally developed by Oak Ridge National Laboratory (ORNL), which serves as the high-power reference for the FHR platform. To accurately capture the neutronic behavior of this complex, heterogeneous geometry, high-fidelity stochastic methods are required. While the OECD/NEA FHR/AHTR Benchmark (Phase II-A) comprises three distinct exercises, the present work focuses exclusively on Exercise 1, [2][3]. This exercise defines a steady-state condition characterized by uniform temperature (948 K) and material density distributions throughout the model. The axial symmetry of the model implies that the exact solution is also axially symmetric which enables quantifying numerical axial tilts in the solution. Lessons learned from evaluating results of Exercise 1 from all participants will be used to finalize

specifications for Exercises 2 and 3, which involve axially varying temperature profiles and control rod insertions. Despite to this narrowed scope, Exercise 1 provides an essential baseline for code-to-code comparison and the verification of spatial and energy-dependent neutronic distributions. The primary objective of this study is to perform a detailed neutronic characterization of the FHR core using the continuous-energy Monte Carlo code Serpent 2.2.3, [5]. This paper reports on the calculation of the effective multiplication factor (k_{eff}), fission rate density (FRD) distributions, and the total and three-group neutron flux distributions. Furthermore, the study examines the behavior of flux uncertainties and assesses symmetry effects to establish a rigorous reference for future benchmark phases.

2 METHODOLOGY

The FHR core model adopted in this analysis is based on a modified ORNL AHTR reference design, with an adjusted active core height and a configuration consisting of 168 hexagonal fuel elements. The resulting geometry necessitated corresponding modifications to the reactor vessel, downcomer, and reflector dimensions to ensure geometric consistency. The fuel elements are arranged with 120° rotational symmetry and utilize uranium oxycarbide (UCO) fuel with a nominal enrichment of 9.0 wt% ^{235}U. The fuel is embedded within graphite plates (planks) as a three-dimensional lattice of TRISO particles, while FLiBe (2LiF–BeF_2) is used as the primary coolant.

Figure 1 shows the horizontal cross-section of the active fuel element. Inter-plank spacing is enforced using support half-cylinders of 0.7 cm radius. Reduced-radius half-cylinders are employed to maintain the spacing between the upper and lower planks of the Y-shaped structure and the outer wrapper. Modelling assumptions and experience acquired during calculation of fuel assembly in benchmark Phase I-C were directly applied to core model development [1][4].

The horizontal cross-section of the FHR core model is shown in Figure 2. The total model height is consistent with the fuel assembly height and, including axial reflector regions, is 550 cm. Fuel elements are arranged in seven radial zones. For the purposes of Exercise 1, the central element and the replaceable radial reflector elements are treated using identical geometric representations to maintain symmetry consistency. Each element consists of a graphite hexagonal prism containing a central coolant channel of 2 cm radius. The control rods and integral fuel burnable absorbers were not modeled.

Axially, each fuel element is subdivided into five distinct regions: the bottom reflector region, the lower non-fueled extruded section (without TRISO particles), the fueled section, the upper non-fueled extruded section (without TRISO particles), and the top reflector region, Figure 3. The upper and lower reflector regions are represented as a homogeneous mixture of graphite and FLiBe coolant with equal volume fractions. Each reflector region is 50 cm in height, whereas the non-fueled sections of the fuel assembly are 25 cm in height. Apart from the reduced axial extent, these regions are geometrically equivalent to the fueled section, with the exception of the absence of fuel stripes.

The fixed portion of the radial reflector is modeled as a monolithic graphite block filling the annular region between the replaceable hexagonal elements and the inner surface of the core barrel, Figure 2. The core barrel is approximated as a graphite cylinder, although it is manufactured from a carbon–carbon composite material; this approximation is adopted for modeling consistency.

The annular region between the reactor vessel and the core barrel contains the downcomer and the reactor vessel liner. The reactor vessel liner and the reactor vessel are assumed to be fabricated from nickel-based alloys, namely alloy Hastelloy N and alloy Incoloy 800H. The first alloy is specifically associated with molten salt reactor development at Oak Ridge National Laboratory. Alloy 800H is included as a representative high-temperature structural alloy widely used in nuclear and industrial systems requiring long-term creep resistance; no specific MSR application is implied.

Neutron transport calculations were performed using Serpent 2.2.3 and ENDF/B-VII.1 cross section library. Thermal scattering data (S(α,β)) were applied to graphite, while they were not applied to FLiBe. The baseline calculation employed 10^5 neutron histories per generation, with 1,000 active and 100 inactive cycles. Fission rate distributions at the fuel assembly level were obtained using

hexagonal tally meshes. Statistical convergence was assessed as a function of both active cycles and particle histories to ensure robust quantification of radial and axial symmetry effects in the modified AHTR geometry. Vacuum boundary conditions were applied in all simulations.

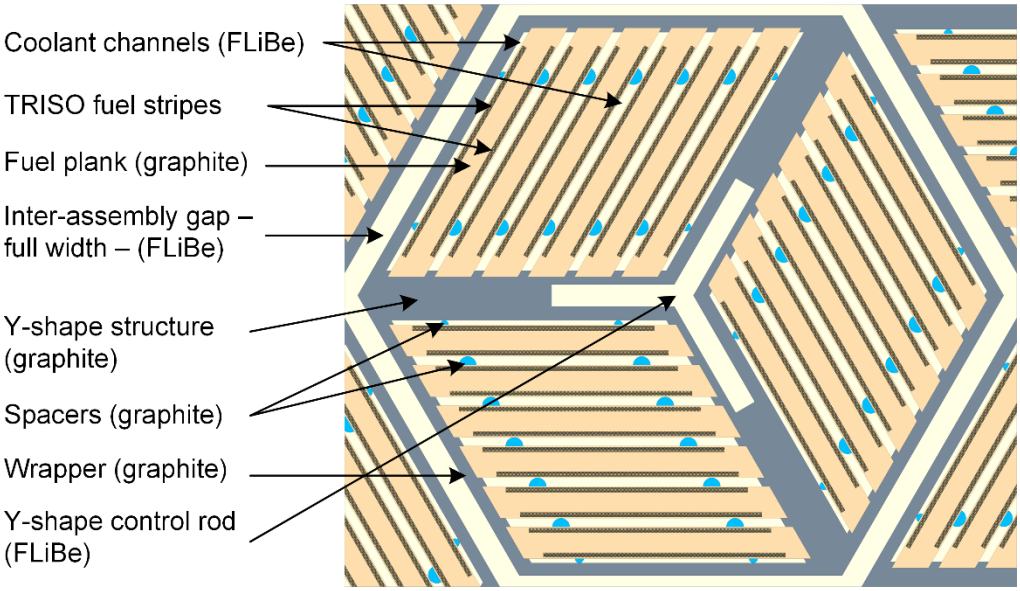

Figure 1: Geometry of fuel assembly as modeled in Serpent2 code

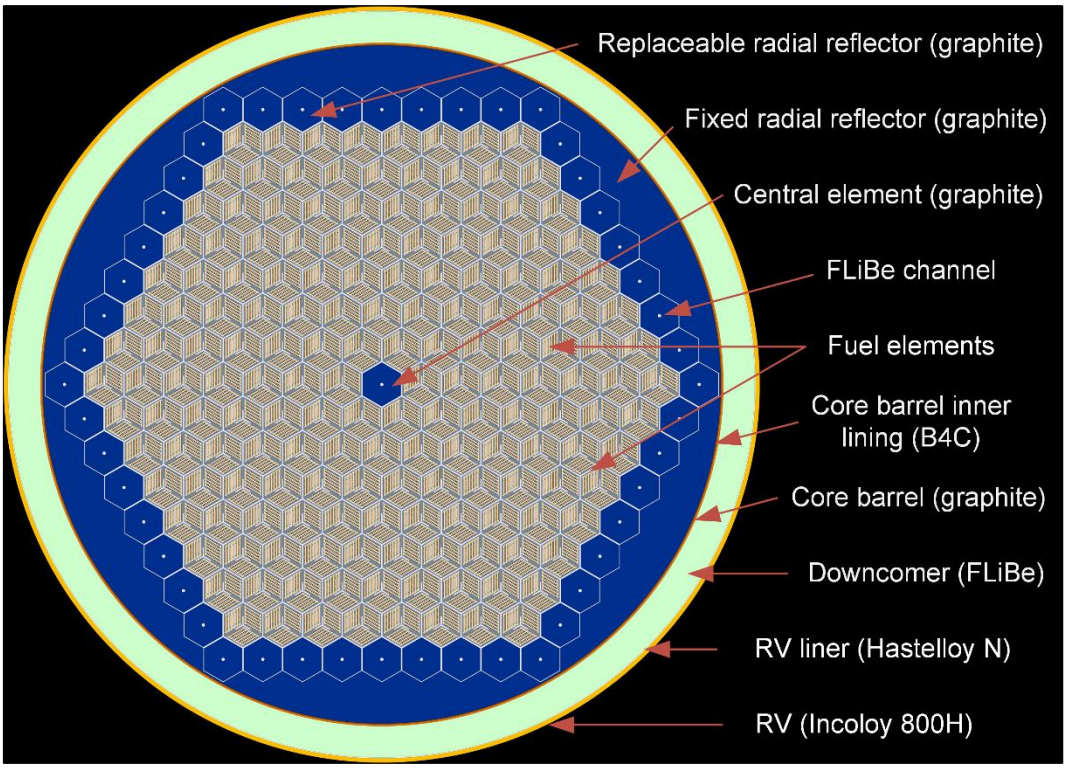

Figure 2: Radial cross section of FHR core as seen by Serpent2 code

The initial calculation (submitted for benchmark comparison) had a mistake in the modeling of replaceable reflector assemblies in core center and at the core periphery. The graphite material was assumed across opening cross section (fuel assembly + inter-assembly gap half width), except in the central cooling hole. That way FLiBe coolant in inter-assembly gap was neglected. The model is called *base* model and new one was called *corrected* model.

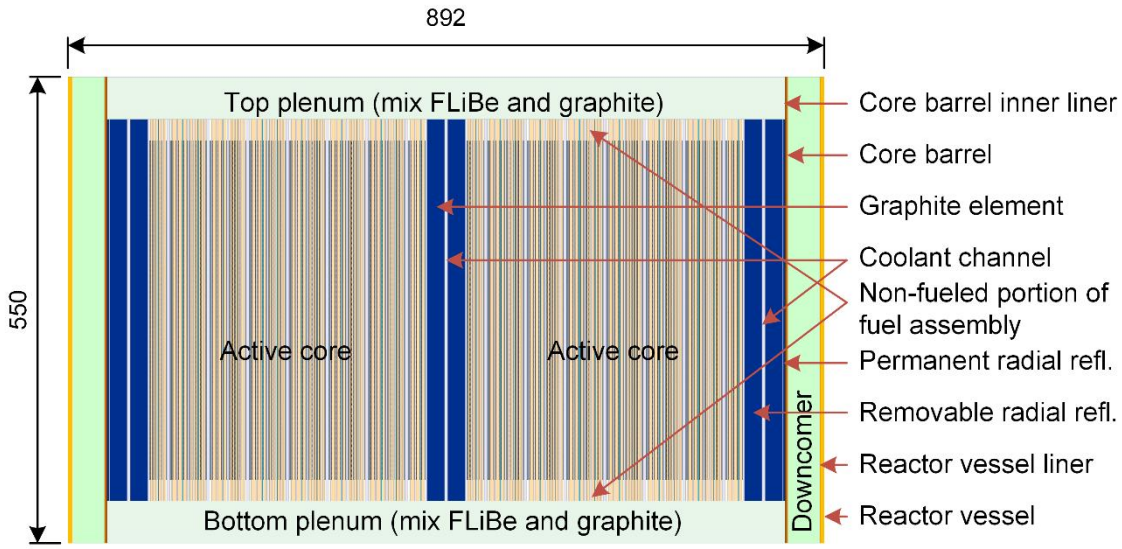

Figure 3: Axial cross section of FHR core in Serpent2 code

3 RESULTS

The calculations were performed for *base* and *corrected* model at 1200 and 2000 active generations (cycles). In all cases number of histories (particles) per generation was 100000 and number of skipped generations was 100. The number of neutrons per fission was 2.43773 and recoverable energy per fission was 202.283 MeV. The last version of Serpent2 code (2.2.3), compiled for Cygwin64 environment within Windows 10 operating system, was used in all calculations on PC equipped with AMD 16 cores CPU. The typical running times were between 17 and 29 hours of wall-clock time.

The first result requested for benchmark comparison is effective multiplication factor, Table 1. The change (increase) in k_{eff} for increased number of generation cycles (from 1200 to 2000) is rather small (6–14 pcm), with expected decrease in statistical uncertainty. The main difference is decrease (around 200 pcm) in multiplication factor when going from *base* to *corrected* model. The *corrected* model is less moderated and has larger absorption in added FLiBe assembly gaps in replaceable reflector assemblies.

The fission rate was tallied for each of the 168 hexagonal fuel assemblies, at 16 equidistant axial locations (active core height of 400 cm). The fission rate was normalized to specified benchmark power density of 200 W/gU. The fission rate density was calculated during postprocessing from fission rates assuming 332.834 cm^3 as active fuel volume of assembly axial segment. The fission rate densities (fissions·cm^{-3}·s^{-1}) for each of 168 Fuel Assemblies (FAs) are shown in Figure 4 for *corrected* model with 2000 active generations. The FAs are labeled using three digits. The first digit denotes the ring number, while the other two digits indicate the assembly numbering within the ring (clockwise, starting from the negative *x*-axis). There are 7 rings, numbered from center toward core periphery, having 6, 12, 18, 24, 30, 36 and 42 assemblies per ring. The rainbow color scheme was used in visualization. The concept of ring was used to organize benchmark results and it is not characteristics of AHTR design. The relative uncertainties of the FA fission rate densities are shown in Figure 5a. The uncertainties are generally small and they are increasing from core center toward core periphery, with maximum at core corners. Figure 5b shows the fuel assembly peak-to-average fission rate densities. The radial distribution is symmetric due to symmetric core geometry and material composition. Maximum peak-to-average value is 1.807 and minimum is 0.409. Core average fission rate density was 6.0837e13 fissions·cm^{-3}·s^{-1} and it is almost the same for all calculation cases. The core relative axial power distribution (calculated from fission density rates) is shown Figure 6. It

is very difficult to see difference between *base* (label c) and *corrected* cases (label d) or influence of number of active cycles (1200 or 2000). The single representative value for axial distribution symmetry is core Axial Offset (AO). It is calculated as ratio of top and bottom core half power difference and total core power. It is usually expressed in percent units. The expected theoretical value for symmetric core should be zero. Calculated values are given in last column of Table 1. We have expected to see that core wide AO decreases toward zero with increased number of generations, but that was not the case. The fuel assembly AOs for the *corrected* 2000 case are shown in Figure 7a. Fuel AO values were dispersed and core wide AO can be small for rather large FA AO values of the opposite sign. Calculated *corrected* 2000 FA AO values are between -0.979 % and 0.991 %. The mean absolute and root mean square (RMS) values of the FA AOs are 0.219 % and 0.277 %, respectively. As expected these values are larger than arithmetic average of FA AOs (core wide AO). Corresponding *corrected* 1200 case minimum and maximum AO values are -1.014 % and 1.040 %, respectively. Mean absolute and RMS values of FA AOs are 0.283 % and 0.363 %. Mean absolute and RMS values of FA AOs are obviously decreasing with increase in number of generations and are more reliable indicator of core AO than min/max values or core wide average AO. The same is true for *base* cases. The *base 2000* case has min/max values between -0.744 % and 0.401 % and mean absolute and RMS values of FA AOs are 0.239 % and 0.290 %. The *base 1200* case has min/max values between -0.640 % and 0.842 % and mean absolute and RMS values of FA AOs are 0.264 % and 0.331 %. The base and corrected cases have generally similar mean absolute and RMS values of FA AOs.

Table 1: Core wide calculation results

Case	k_{eff} ()	k_{eff} uncertainty ()	Core AO (%)
Base 1200	1.36011E+00	4.9E-05	0.1248
Base 2000	1.36017E+00	3.8E-05	-0.207
Corrected 1200	1.35827E+00	4.9E-05	0.0076
Corrected 2000	1.35841E+00	3.8E-05	0.048

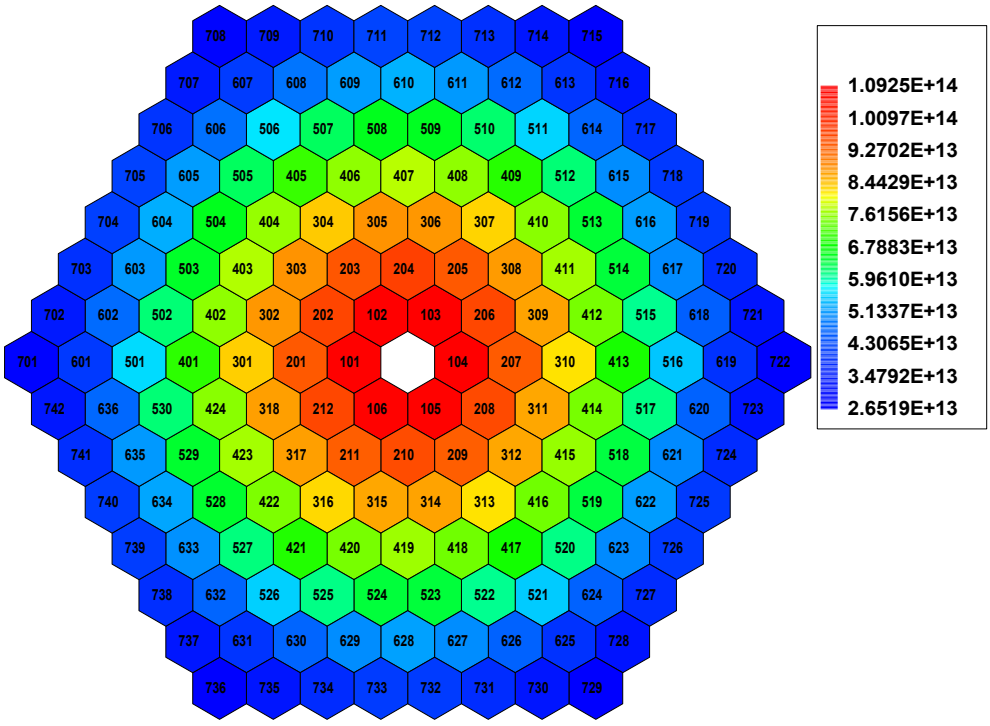

Figure 4 Fission rate densities for core fuel assemblies (fissions·cm^{-3}·s^{-1}), *corrected* 2000 case

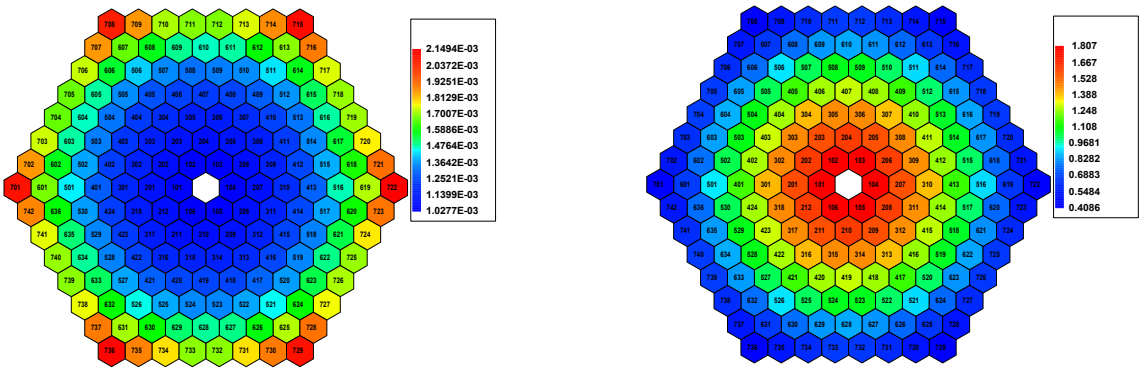

a b

Figure 5 Relative uncertainty of fission rate density (a) and peak-to-average fuel assembly values (b), *corrected* 2000 model

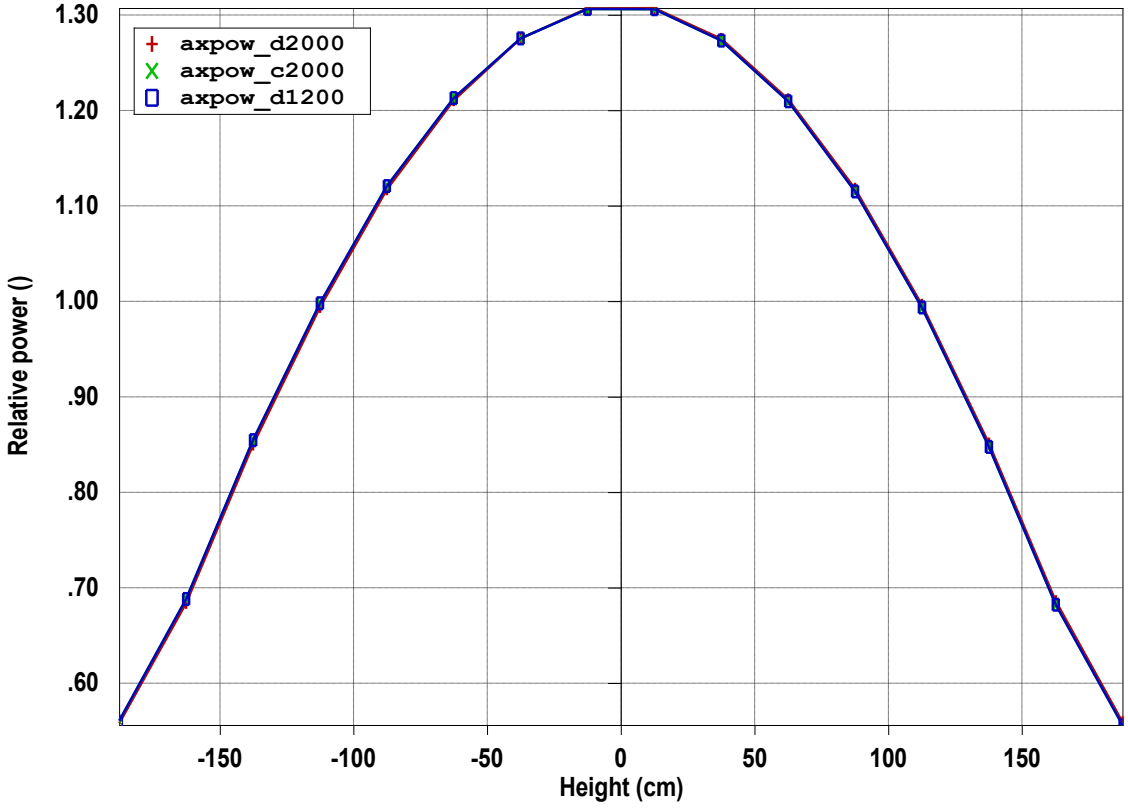

Figure 6 Axial distribution of core relative power

Table 2: Region peak-to-average FRD values

	Peak-to-average region FRD			
Region	Base 1200	Base 2000	Corrected 1200	Corrected 2000
1	1.7888	1.7873	1.7891	1.8059
2	1.5653	1.5652	1.5842	1.5953
3	1.4084	1.4082	1.4325	1.4361
4	1.2228	1.2229	1.2428	1.2428
5	1.0134	1.0137	1.0224	1.0199
6	0.7871	0.7868	0.7799	0.7771
7	0.5964	0.5967	0.5689	0.5660

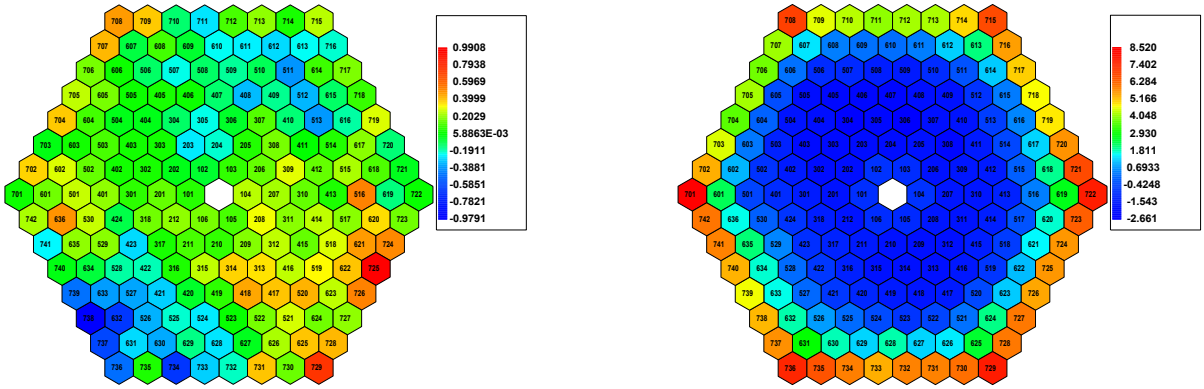

a b

Figure 7 AO (%) per fuel assembly for the *corrected* 2000 model (a), and relative difference (%) between the base and *corrected* 2000 case FA fission rate densities (b)

Peak-to-average region fission rate density values are shown in Table 2. The influence of number of generations is rather small. *Corrected* cases have generally lower peripheral peak-to-average values what is related to the introduced FLiBe inter-assembly gaps. That can be seen in Figure 7b too. The relative difference is defined as (Base 2000 FRD – Corrected 2000 FRD)/(Corrected 2000 FRD)×100 %. Base cases have higher absolute and relative fission rate densities at the periphery (and very similar core average FRD). The axial distributions of ring averaged fission rate densities are shown in Figure 8. The distributions are symmetric and with the values decreasing from center toward core periphery.

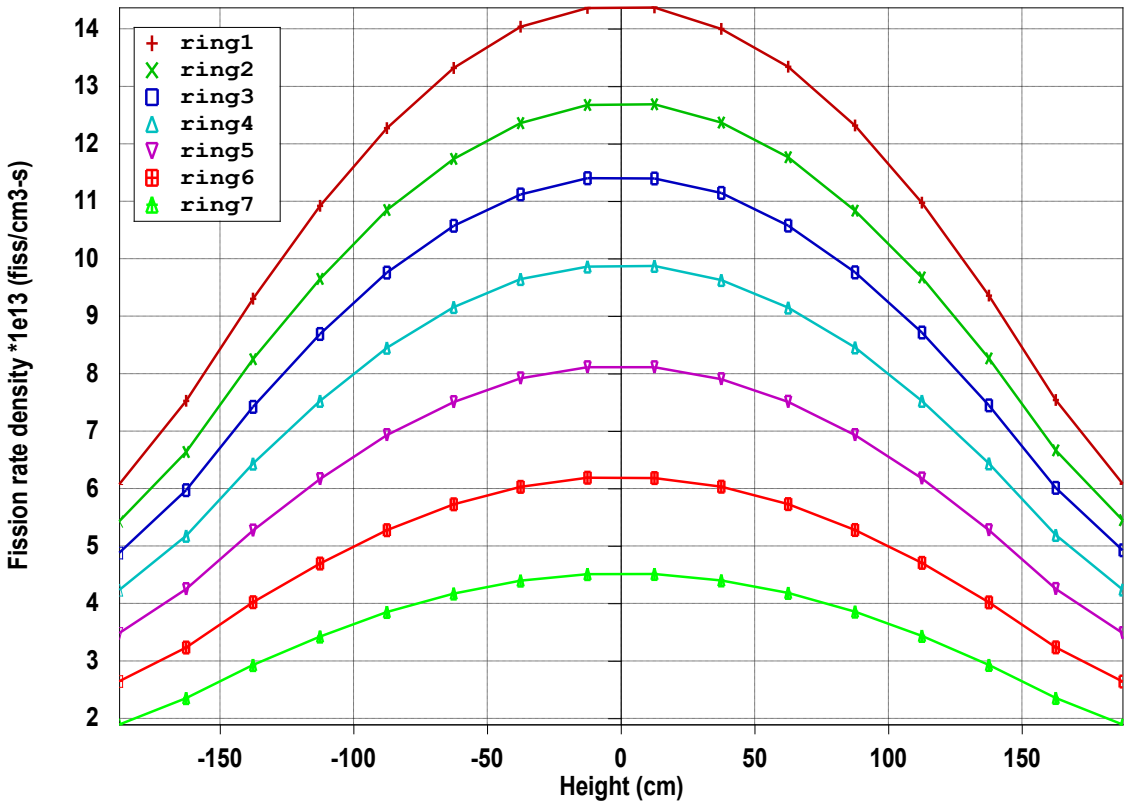

Figure 8 Axial distribution of ring averaged fission rate densities, *corrected* 2000 case

The neutron flux energy spectrum was tallied for a cube with sides 400 × 400 × 400 cm and for prescribed energy structure using 252-group SCALE Library group boundaries. The energy

dependence of neutron flux per unit lethargy was plotted in Figure 9. The clear peak in thermal energy range can be seen. The *base* (label before) and *corrected* case (label after correction) have very similar results with small difference near thermal peak.

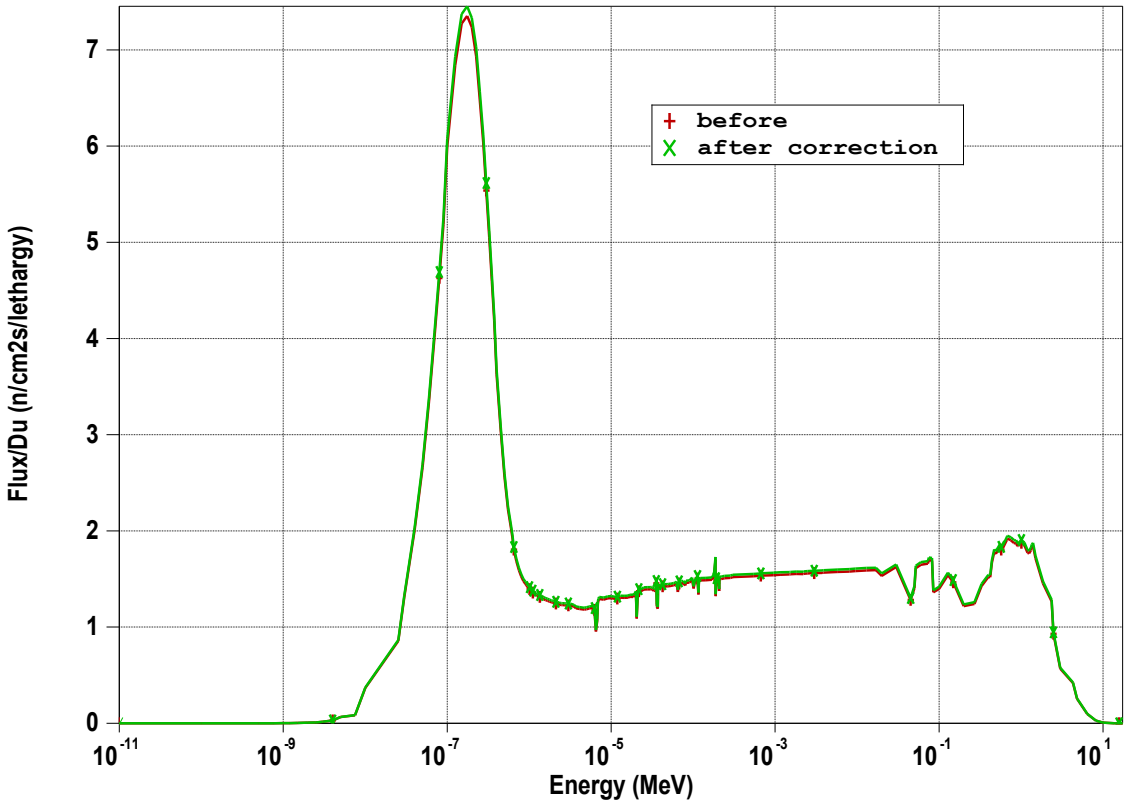

Figure 9 Flux per unit lethargy spectrum for initial model and for model after correction

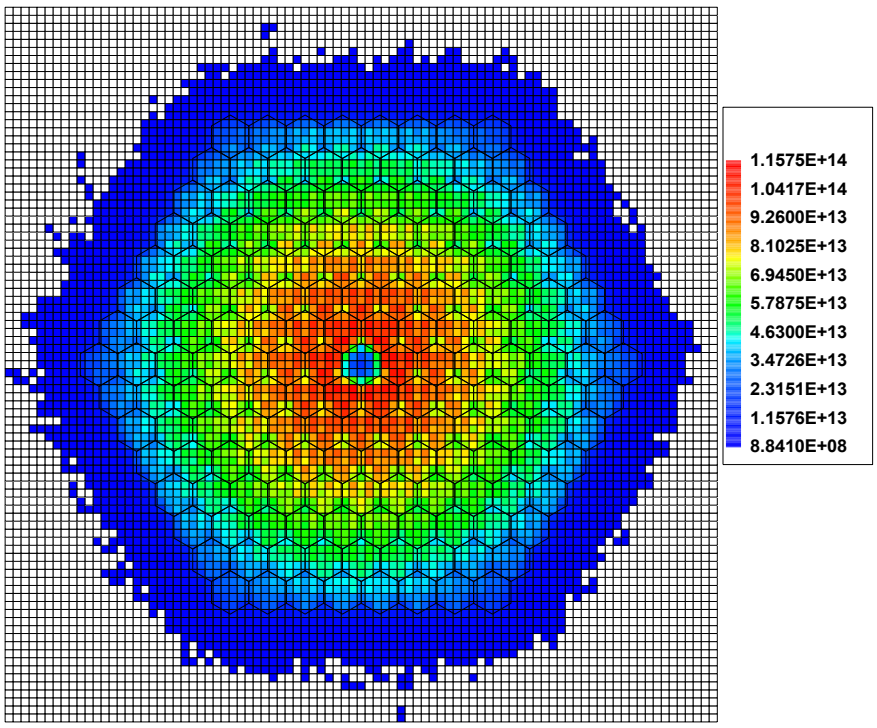

Figure 10 Neutron flux (n/cm^2·s) radial distribution with outlier values at the periphery for energy group 3 and axial layer 28, *corrected* 2000 case

According to the benchmark specification, the neutron flux is tallied for volume dimensions from −445 to +445 cm in the *x*- and *y*-directions, and from −275 to +275 cm in the *z*-direction. The three-group energy structure has boundaries 1.000E-11, 3.000E-06, 1.000E-01, and 2.000E+01 MeV. The bins are based on *x*, *y*, *z* discretization of 89 × 89 × 55 mesh, giving homogenous mesh cells with cell (voxel) dimension of 10 × 10 × 10 cm. The *x*–*y* results are requested in axial plane number 28 and *x*–*z* results are for the *y*-plane layer 45. Due to statistical nature of Monte Carlo results some cells are having numerical noise (outliers) when number of active generations is not large enough. The neutron flux distribution in central *x*–*y* plane for thermal energy group (group 3) is shown in Figure 10. From the legend it is clear that some flux values (outliers) are for three orders of magnitude lower than others. In order to remove such cells the postprocessing of the results was performed to remove all cells having uncertainties larger than 10 %.

In Figure 11 neutron flux distributions are shown for central *x*–*y* plane (*z*-layer 28) for fast group (a), epithermal (b) and thermal (c) groups, for *corrected* 2000 case. In part (d) of the figure total flux is shown. The original group results were integrated in given energy range during postprocessing and related uncertainties were calculated. When we have directly tallied energy integrated flux, very similar results were obtained. Spatial and energy dependence of neutron flux is as expected. In the figures hexagonal shapes of the fuel assemblies are overlaid on the *x*–*y* mesh.

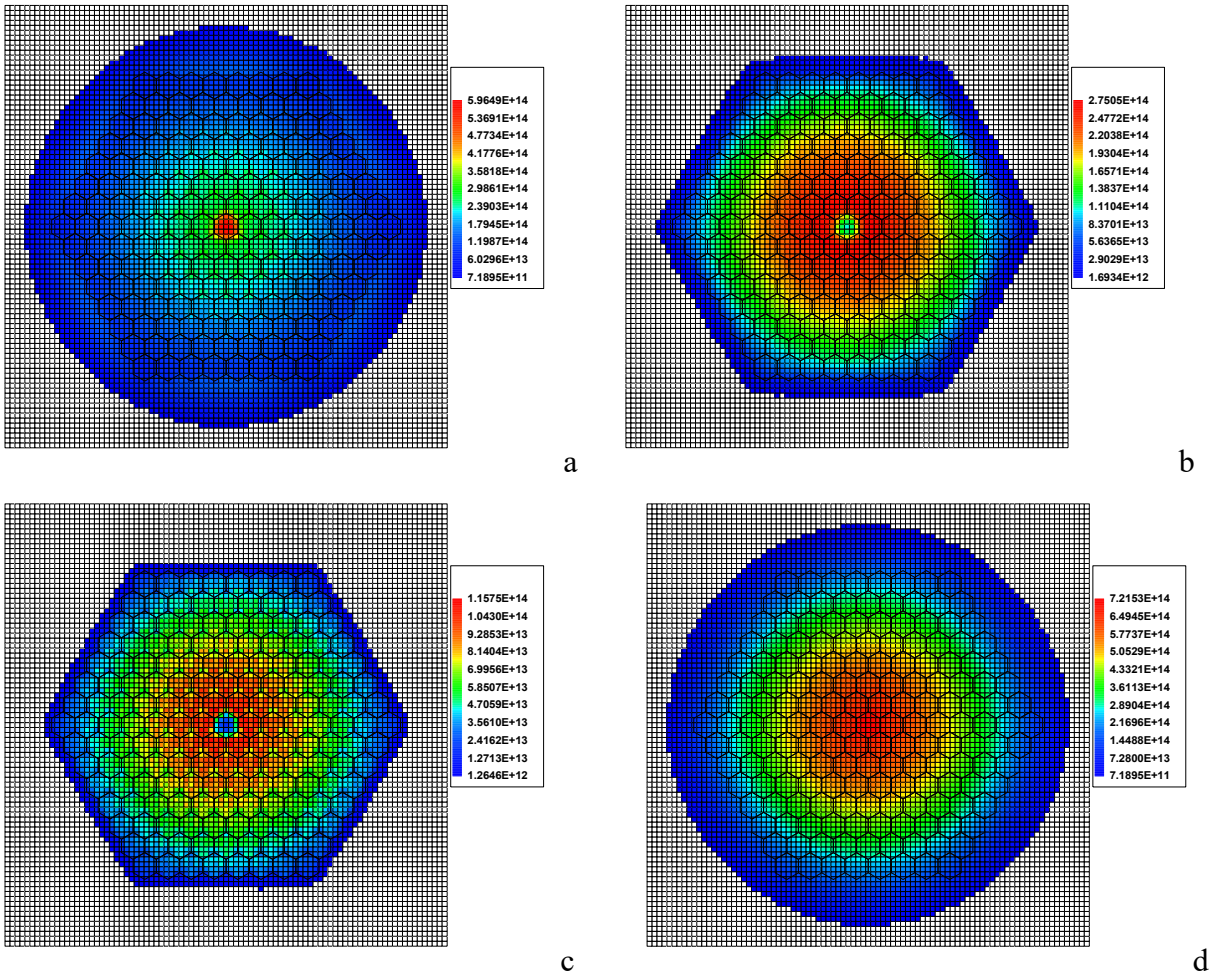

Figure 11 Flux distribution (n/cm^2·s) in central *x*–*y* plane, *corrected* 2000 case, fast energy group (a), epithermal group 2 (b), thermal group (c), and total flux (d)

Similarly, in Figure 12 neutron flux distributions are shown for central *x*–*z* plane (*y*-layer 45) for fast group (a), epithermal (b) and thermal (c) groups, for *corrected* 2000 case. In part (d) of the

figure total flux is shown. The characteristic role of the central reflector channel can be seen in different energy ranges.

3D distributions of flux relative uncertainty are shown in Figure 13 for fast group (a), epithermal (b) and thermal (d) groups, for *corrected* 2000 case. In part (c) of the figure the quarter of fast flux relative uncertainty 3D distribution is shown. Only volume voxels with uncertainty values less than 2 % are shown. The uncertainty increases toward periphery and with energy decrease. That means that part of the core volume with uncertainties less or equal 2 % decreases with neutron energy (group increase), what can be seen in the figure.

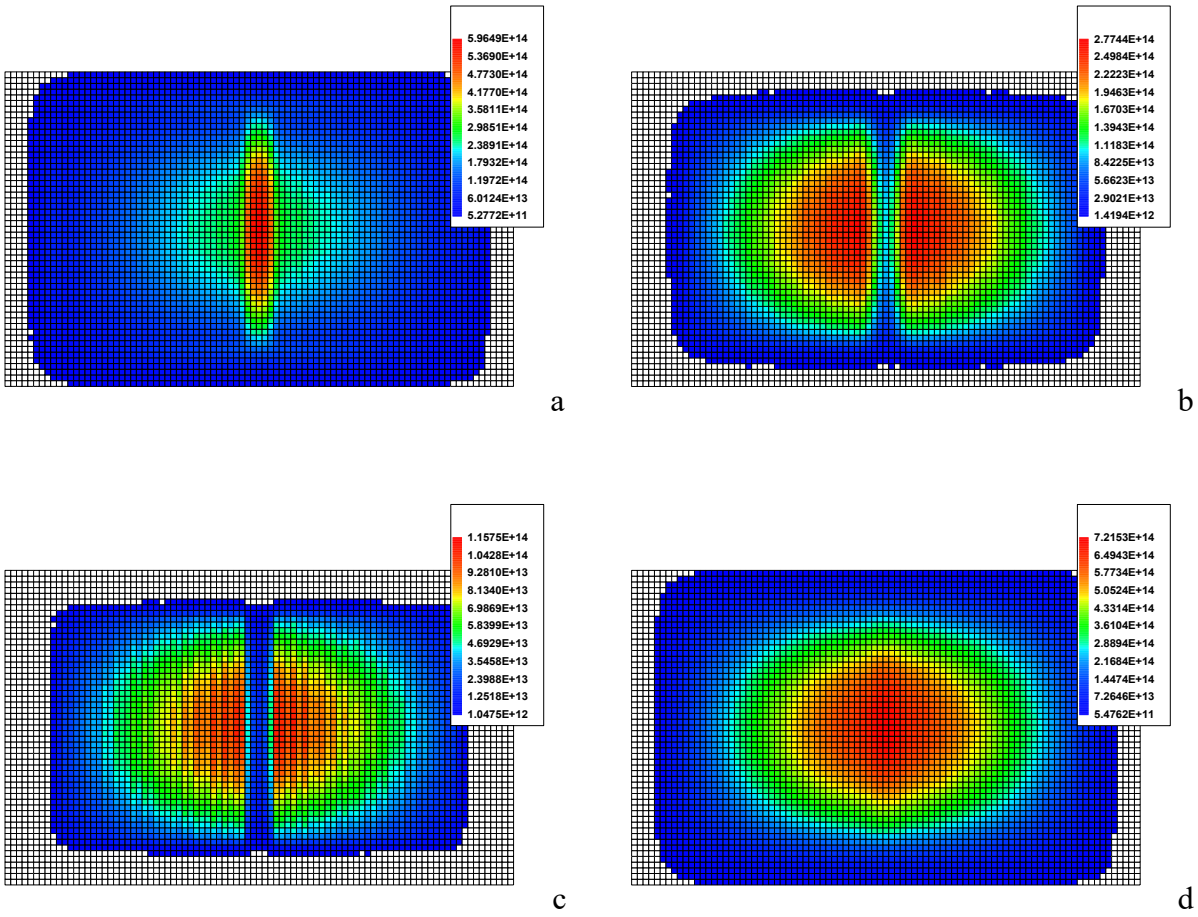

Figure 12 Flux distribution (n/cm^2-s) in central *x–z* plane, *corrected* 2000 case, fast energy group (a), epithermal group (b), thermal group (c), and total flux (d)

Obtained benchmark results are mostly as expected except AO results at fuel assembly level. Taking into account rather complicated geometry of the reactor and at least double heterogeneity of the problem including TRISO particles it is difficult to conclude on overall acceptability of the results before seeing the results of other participants. The original intention of the benchmark is verification of the predictions using code-to-code comparison and statistical evaluation of the results.

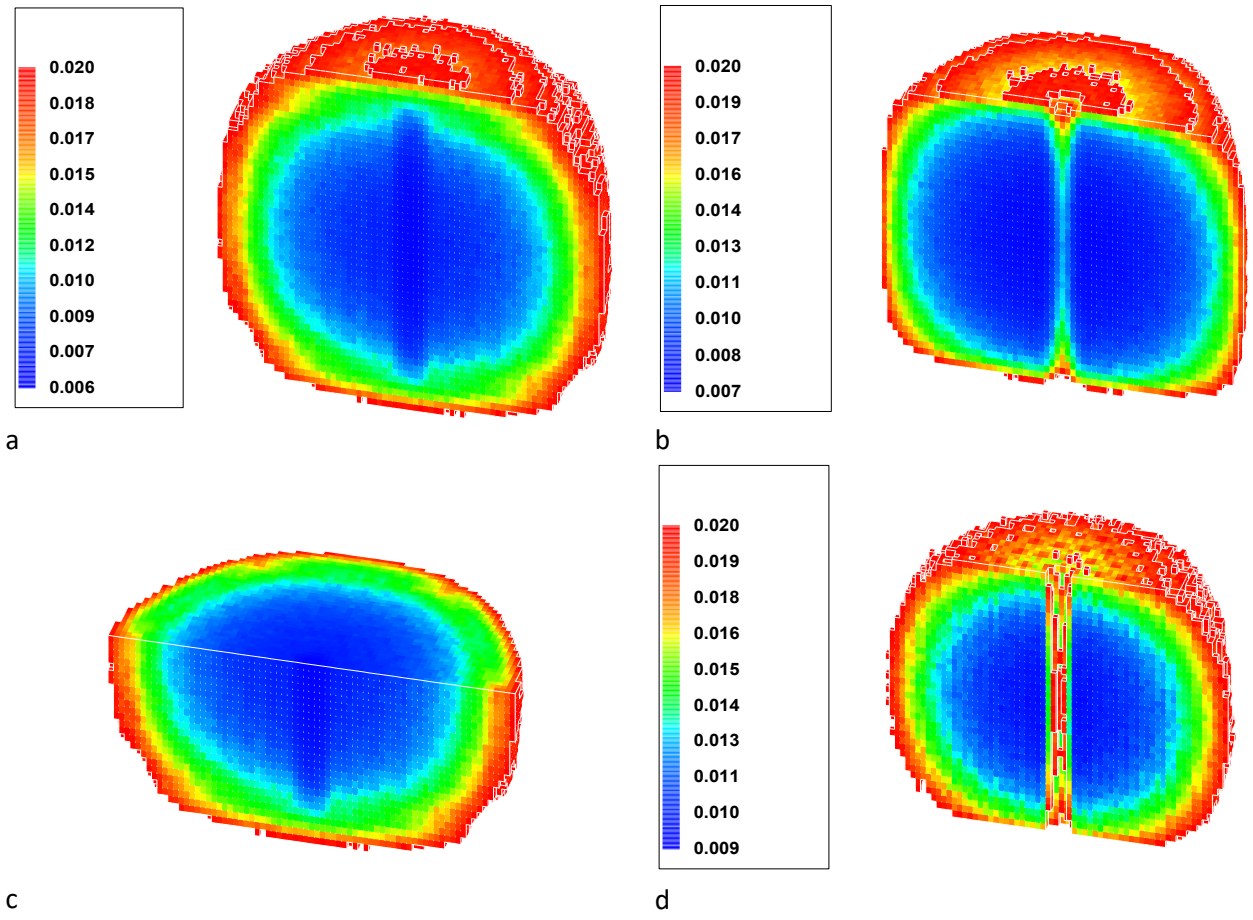

Figure 13 3D distribution of flux relative uncertainty for voxels with value less than 2 %, fast flux (a) and (c), epithermal flux (b) and thermal flux (d), *corrected* 2000 case

4 CONCLUSION

In this paper initial results of OECD NEA FHR/AHTR Benchmark – Phase II-A were shown. The results were checked from the point of view of axial (both core and fuel assembly) and radial flux symmetry. Spatial and energy collapsing of flux results was done both externally using data processing and internally using different sampling criteria in detector definitions.

Obtained results are mostly as expected except for the AO results at fuel assembly level. That results were showing random behaviour hidden by overall reasonable core wide AO. Due to a mistake in model preparation, we had the opportunity to analyse the influence of FLiBe coolant presence in inter assembly gap of replaceable reflector elements at the core periphery. That presence caused a decrease in multiplication factor and a decrease of power in peripheral fuel assemblies compared to the original calculation where the gap was assumed to be graphite.

All calculations were performed using the Monte Carlo neutron transport code Serpent 2.2.3 and it was proven to be a reliable and versatile calculation tool for parallel multicore processing in MS Windows environment.

Taking into account the number of requested results, the postprocessing is rather challenging task and that will be even more true for the benchmark organizer when the results of all participants should be processed.

Due to the rather complicated geometry of the reactor including TRISO particles and due to related cross section processing, it is difficult to conclude on overall acceptability of the results before examining the results of other benchmark participants. Given the lack of any experimental

measurements, the original intent of the benchmark was to verify the predictions using code-to-code comparison and statistical evaluation of the results, for the FHR/AHTR reactor concept.

REFERENCES

[1] B. Petrovic and J. Faulkner, "FHR/AHTR Benchmark, Phase I-C Draft Specifications," Georgia Institute of Technology, Atlanta, Georgia, USA, Tech. Rep., Nov. 7, 2022.

[2] B. Petrovic and J. Faulkner, "FHR/AHTR Benchmark Phase II-A Specifications (Rev. 0)," Georgia Institute of Technology, Atlanta, Georgia, USA, Tech. Rep., Aug. 18, 2025.

[3] B. Petrovic and J. Faulkner, "FHR/AHTR Benchmark Update, Phase II-A," Georgia Institute of Technology, Atlanta, Georgia, USA, Tech. Rep., Dec. 16, 2025, updated Jan. 9, 2026.

[4] B. Petrovic, J. Faulkner, K. M. Ramey, et al., "Fluoride-salt High-temperature Reactor (FHR) NEA Benchmark Phase I-C: Results and Lessons Learned," in *Proc. Int. Conf. Physics of Reactors (PHYSOR 2026)*, Torino, Italy, Apr. 19–23, 2026.

[5] J. Leppänen, V. Valtavirta, A. Rintala, and R. Tuominen, "Status of the Serpent Monte Carlo code in 2024," *EPJ Nucl. Sci. Technol.*, vol. 11, no. 3, 2025, doi: 10.1051/epjn/2024031

[6] K. M. Ramey and B. Petrovic, "Monte Carlo modeling and simulations of AHTR fuel assembly to support V&V of FHR core physics methods," *Ann. Nucl. Energy*, vol. 118, pp. 272–282, 2018, doi: 10.1016/j.anucene.2018.04.003

[7] K. M. Ramey and B. Petrovic, "Assessment of modeling decisions for depletion multiphysics studies of AHTR," *Nucl. Sci. Eng.*, vol. 199, no. 11, pp. 1934–1953, 2025, doi: 10.1080/00295639.2025.2464460